

# Thermalization of dense hadronic matter in Au + Au collisions at energies available at the Facility for Antiproton and Ion Research

Somnath De<sup>1</sup>, Sudipan De<sup>2</sup>, and Subhasis Chattopadhyay<sup>3</sup>

<sup>1</sup> *Institute of Physics, Bhubaneswar, Odisha, India*

<sup>2</sup> *Universidade de São Paulo, São Paulo, Brasil and*

<sup>3</sup> *Variable Energy Cyclotron Centre, 1/AF, Bidhan Nagar, Kolkata, India*

The conditions of local thermodynamic equilibrium of baryons (non-strange, strange) and mesons (strange) are presented for central Au + Au collisions at FAIR energies using the microscopic transport model UrQMD. The net particle density, longitudinal-to-transverse pressure anisotropy and inverse slope parameters of the energy spectra of non-strange and strange hadrons are calculated inside a cell in the central region within rapidity window  $|y| < 1.0$  at different time steps after the collisions. We observed that the strangeness content is dominated by baryons at all energies, however contribution from mesons become significant at higher energies. The time scale obtained from local pressure (momentum) isotropization and thermalization of energy spectra are nearly equal and found to decrease with increase in laboratory energy. The equilibrium thermodynamic properties of the system are obtained with statistical thermal model. The time evolution of the entropy densities at FAIR energies are found very similar with the ideal hydrodynamic behaviour at top RHIC energy.

PACS numbers: 25.75.-q, 25.75.Dw, 51.30.+i, 12.40.Ee

## I. INTRODUCTION

The motivation of the relativistic heavy ion collider experiments is to explore the properties of strongly interacting matter (partonic or hadronic) at the finite temperature and/or density. The current heavy ion research facilities e.g; Relativistic Heavy Ion Collider (RHIC) and Large Hadron Collider (LHC) are focused in unveiling the properties of deconfined quark-gluon matter created at the extreme temperature and almost vanishing net baryon density [1, 2]. At this regime the lattice quantum chromodynamics (lQCD) simulations have reported a crossover from hadronic to partonic phase and the existence of critical point where the first order phase transition line terminates [3]. Thus RHIC has initiated the beam energy scan program to find the location of critical point in the QCD phase diagram (temperature (T)- baryo-chemical potential ( $\mu_B$ ) plane) [4].

In contrary to the above experiments, the future Compressed Baryonic Matter (CBM) experiment at FAIR / GSI laboratory is aimed to explore another facet of QCD phase diagram; at high baryon density ( $\sim 7 - 8$  times ground state nuclear matter density) and moderate temperature [5, 6]. The experiment would be playing a very significant role in the scientific quest of understanding the behaviour of QCD at high density regime. The facility is being designed to collide various species of heavy ions at fixed target mode with the anticipated beam energies 5-45 GeV/nucleon. The diagnostic probes of the matter created in the collisions include; (i) Short lived vector mesons ( $\rho$ ,  $\omega$ ) decaying to dilepton pairs, (ii) Production of multi-strange hyperons ( $\Xi$ ,  $\Omega$ ) (iii) Dissociation of Charmonium ( $J/\Psi$ ) and charmed hadron

( $D$ ,  $\Lambda_c$ ) states, etc. The existence of first order phase transition from hadronic to partonic matter and restoration of chiral symmetry at the large  $\mu_B$  is expected to be found from the FAIR energy scan program [7]. Earlier experiments such as; RHIC-AGS and CERN-SPS were aimed to explore above features through the measurement of bulk observables like; flow and momentum spectra of hadrons. However their efforts were constrained due to limited beam luminosity. In recent years a similar research program (NICA) at JINR-Dubna has been proposed to explore phases of nuclear matter at high baryon density [8]. But the CBM experiment would be more efficient for the detection of bulk and rare probes, with the availability of high intensity ion beams [9].

In order to compute the dynamic evolution of the matter created in such collisions, we need macroscopic/microscopic models. The macroscopic models like; hydrodynamics rely upon the assumption of local thermal equilibrium of the created matter on a certain time scale. The actual thermalization criterion has seldom been tested. There are a few works, addressed the issue at higher collision energies in the framework of perturbative QCD [10] or color-glass condensate theory [11]. On the other hand microscopic Monte Carlo models like: UrQMD [12], HSD [13], AMPT [14] work on the postulated interaction among it's constituents (parton, hadron, or string) and does not require any assumption of local thermal equilibrium. Therefore, it is very important to test whether the dense baryonic matter created in these collisions achieve a local thermal equilibrium or not. In particular, we have investigated the time-scale of local thermal equilibration of non-strange and strange baryons in an elementary volume in phase-space from the time evolution of

longitudinal-to-transverse pressure anisotropy and slope of the energy spectrum. For this purpose, we have employed the microscopic, N-body transport model called Ultra-relativistic Quantum Molecular Dynamics (UrQMD). A comparison between the model and the data for central Pb+Pb collisions at different energies at CERN-SPS can be found in Ref. [15]. We considered the most central collisions of gold (Au) nuclei at four beam energies associated with the CBM experiment. The incident beam energy has obvious implication on the time-scale of equilibration, which can be found in the subsequent section.

The organization of the paper goes as the following. In the next section, we briefly recapitulate about the microscopic transport model UrQMD and then discuss about the methodology of our analysis. In section 3, we show the results for the time evolution of density, ratio of longitudinal-to-transverse pressure and inverse slope parameter of the energy spectra for non-strange baryons, strange baryons and strange mesons. In section 4, we have utilized the statistical thermal model to extract the post-equilibrium thermodynamic parameters e.g., temperature, chemical potentials and calculated the entropy density of the system. Finally we have summarized the findings in section 5.

## II. METHODOLOGY OF THE ANALYSIS

The model UrQMD has been extensively used in recent years for describing heavy ion collisions of center of mass energy ranging from few GeV/nucleon to few TeV/nucleon [12]. We used the UrQMD-version:3.3p2 in default cascade mode without invoking any hydrodynamic evolution for the initial state. It includes 55 baryon species (up to mass 2.25 GeV) and 32 meson species (up to mass 1.9 GeV) and their corresponding anti-particles and iso-spin projected states. Particle production in UrQMD occurs through inelastic collisions, decay of meson, baryon resonances, and string fragmentation mechanism. At low energies ( $E_{\text{lab}} < 4$  GeV) hadronic interactions are based on two body or three body potential. However at high energies, hadron-hadron collisions are performed stochastically in the spirit of cascade model [16]. The total (elastic and inelastic) cross-sections of baryons and mesons are generally fitted to experimental proton-proton or proton-pion scattering data. For the resonant baryon-meson or hyperon-baryon scattering where no experimental data are available, principle of detail balance or additive quark model have been used. The resonance scattering dominates the total cross-section at low beam momenta (upto  $p_{\text{lab}} \sim 2$  GeV) however towards higher beam momenta string ex-

citation has the largest contribution. The inelastic collisions and decays are responsible for changing the particle abundances of the system while the elastic collisions modify the momentum distribution of hadrons.

We have considered central collisions (impact parameter  $b = 2$  fm) of Au nuclei at the laboratory energies ( $E_{\text{lab}}$ ) 10A, 20A, 30A, 40A GeV. For each energy we ran the simulation at different time steps ranging from 1fm/c to 15 fm/c.  $6 \times 10^4$  events have been analyzed for each time step. The center of mass frame is chosen as the computational frame in our analysis. We have considered a cell of dimension  $2 \times 2 \times 2$  fm<sup>3</sup> about the origin of Au + Au system. The test volume has been chosen such that the effect of collective flow of the system on the observables will be minimum and at the same time the particle number should be large enough for reasonably small fluctuation in the observables. Additionally a momentum rapidity cut  $|y_{cm}| < 1.0$  has been imposed on the particles under consideration to ensure that the beam nucleon contribution does not come into account. We have calculated the net particle density, different components of microscopic pressure for non-strange baryons, strange baryons and mesons inside the cell. The non-strange baryons include Proton ( $p$ ) and Neutron ( $n$ ), the strange baryons include Lambda ( $\Lambda$ ), Sigma ( $\Sigma$ ), Cascade ( $\Xi$ ), Omega ( $\Omega$ ) and the strange mesons include Kaons:  $K^+$ ,  $K^0$ . All the higher mass resonances (baryon and meson) are allowed to decay. We did not include  $\Omega$  in the pressure calculation at  $E_{\text{lab}} = 10A$  and  $20A$  GeV due to its limited statistics at lower energies. However we expect that inclusion of  $\Omega$  does not modify any conclusion drawn in this work. We have also calculated the energy spectra ( $\text{EdN}/d^3p$  vs.  $E$ ) of Protons and Lambdas inside the cell. Lastly the above quantities are statistically averaged over the number of events for each time step.

## III. RESULTS

### A. Time evolution of net particle density

The time ( $t$ ) is the elapsed time in center of mass frame. Time  $t = 0$  fm/c corresponds to the moment when two nuclei touch each other. The net particle density  $\rho(t)$  is defined as the difference of particle density and anti-particle density. The evolution of net non-strange baryon density ( $\rho_B^{NS}$ ), net strange baryon density ( $\rho_B^S$ ), net kaon density ( $\rho_M^S$ ), and net strange baryon to kaon ratio ( $\rho_B^S/\rho_M^S$ ) are depicted in Fig. 1 at  $E_{\text{lab}} = 10A, 20A, 30A, 40A$  GeV. The net particle density starts from a small value, reaches a maximum around  $t = 2R/(\gamma_{cm}v_{cm})$  when the two nuclei pass through each other and

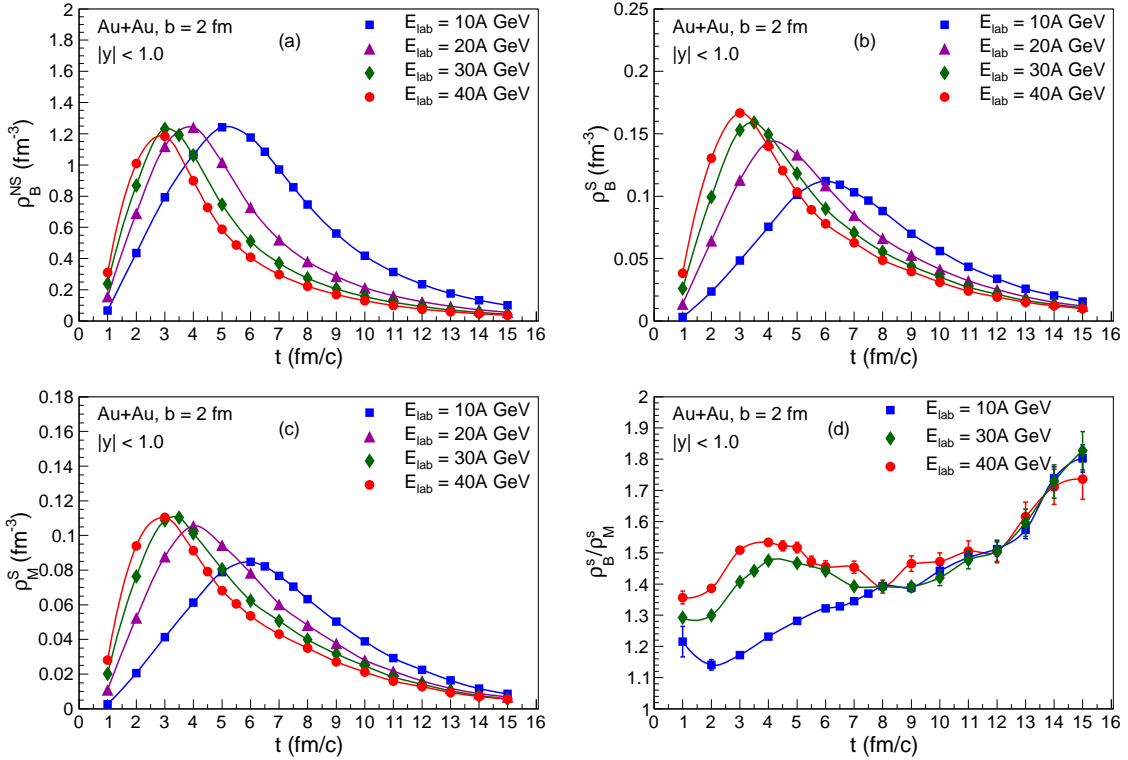


FIG. 1: (Color online)(Upper panel) Time evolution of net density of (a) non-strange baryons ( $\rho_B^{NS}$ ), (b) strange baryons ( $\rho_B^S$ ), (Lower panel) (c) kaons ( $\rho_M^S$ ) and (d) net strange baryon to kaon ratio ( $\rho_B^S / \rho_M^S$ ) inside the central cell for Au + Au collisions ( $b = 2$  fm) at the laboratory energies 10A, 20A, 30A, 40A GeV. The error bars are statistical only.

then falls down as the system expands. The generic feature has been found in agreement with earlier works [17, 18]. Here  $R$  is the radius of Au nucleus,  $\gamma_{cm}$  and  $v_{cm}$  are the Lorentz boost and velocity in center of mass frame. Thus we found the maximum matter density near 6 fm/c at 10A GeV and 3 fm/c at 40A GeV for all species. The production of non-strange baryons has been found almost similar for all the beam energies, but the strange baryon and meson production becomes larger with increasing beam energy. This is probably because of the fact that string excitation mechanism has major contribution to strangeness production at higher energies. The peak of baryonic (non-strange and strange) matter density has been found at 40A GeV, which is about 7–8 times the ground state nuclear matter density. The time evolution of strange baryon to meson ratio has clearly shown the net strangeness content of the created matter is dominated by baryons for all the beam energies. The ratio has been found to grow with time because the kaons and Lambdas are produced through same strong interaction. However the kaons have suffered less scatterings in the medium due to its small interaction cross-section

with other hadrons [19], thus escapes the reaction volume quickly. The production of kaons is larger at higher beam energies can be seen from the non-monotonous behaviour of the ratio at smaller times.

## B. Isotropization of pressure components of baryons and mesons

We have studied the isotropization of different components of microscopic pressure of non-strange baryons, strange baryons and kaons for an expanding system. The pressure components are highly anisotropic immediately after the collision. Thermal equilibrium is established in the cell when they have become nearly isotropic. Different components of microscopic pressure are calculated in UrQMD using ideal gas ansatz [20]:

$$P_{(x,y,z)} = \sum_i \frac{p_i^2(x,y,z)}{3V(p_i^2 + m_i^2)^{\frac{1}{2}}}, \quad (1)$$

where,  $p_i$  is the momentum,  $m_i$  is the mass of  $i$ 'th hadron and  $V$  is the volume of the cell under con-

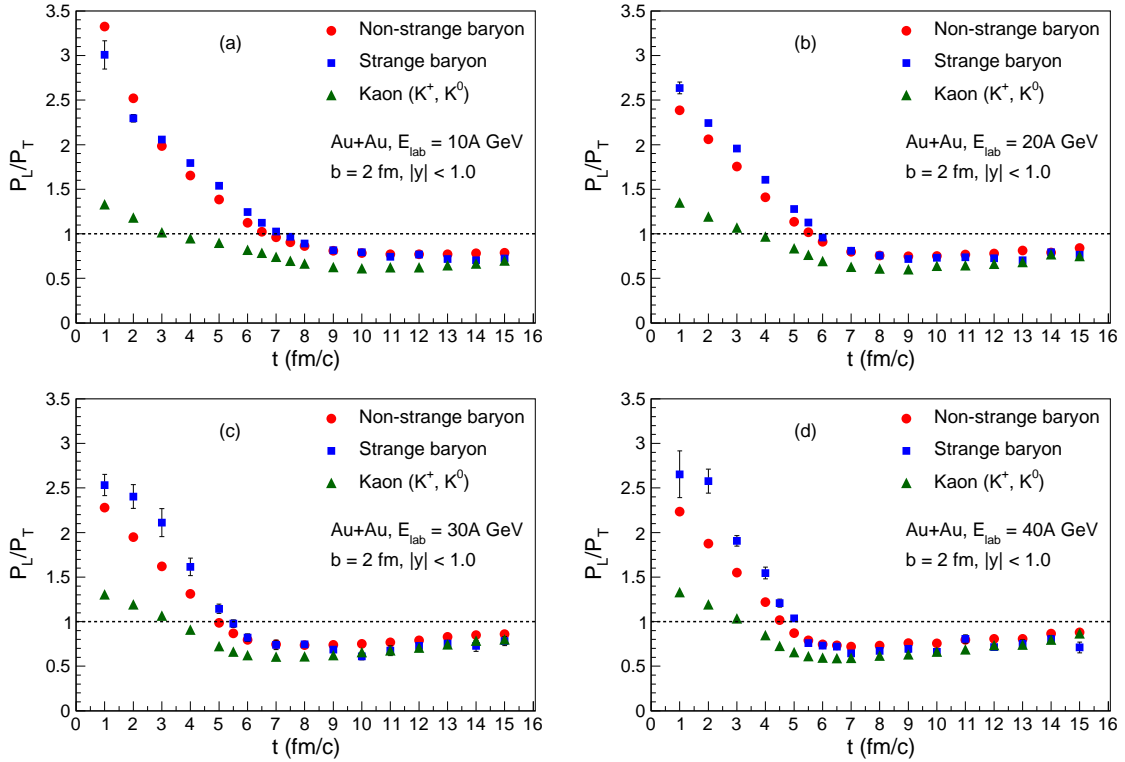


FIG. 2: (Color online) Time evolution of longitudinal-to-transverse pressure ratio ( $P_L/P_T$ ) of non-strange baryons, strange baryons, kaons inside the central cell for Au + Au collisions ( $b = 2$  fm) at the laboratory energies (a) 10A, (b) 20A, (c) 30A, (d) 40A GeV. The error bars are statistical only.

sideration. The longitudinal and transverse components of pressure for an ensemble of hadrons are defined as:

$$P_L = \langle P_z \rangle; \quad P_T = \frac{1}{2}(\langle P_x \rangle + \langle P_y \rangle), \quad (2)$$

here the  $\langle \dots \rangle$  corresponds to the statistical average over the number of events. The time evolution of the longitudinal-to-transverse pressure ratio ( $P_L/P_T$ ) for the above mentioned hadron species are shown in Fig. 2 at the four beam energies.

The  $P_L/P_T$  ratio of baryons (non-strange and strange) starts from a large value at initial times, ultimately settles down to a value close to 1.0. This reflects the longitudinal ( $z$ ) and transverse ( $x, y$ ) momentum distribution of baryons are highly anisotropic at initial times. Successive elastic scatterings in the medium have made their momentum distribution nearly isotropic. We found that the ratio  $P_L/P_T$  becomes 1.0 around 6.5 fm for non-strange baryons and 7 fm for strange baryons at  $E_{\text{lab}} = 10$  A GeV. However the system further evolves and the ratio reaches a constant value  $\sim 0.8$  for  $t \geq 9$  fm/c. At this point we may say that the baryonic matter achieves a thermal equilibrium. Earlier work at AGS energy had also found similar time

scale [20]. The deviation of  $P_L/P_T$  from unity after-equilibrium, is possibly arising due to finite shear viscosity of the hadronic matter [21]. The ratio is more closer to unity as the system approaches towards ideal fluid limit. This has been shown by a recent study on the pressure isotropization in quark-gluon plasma for Au + Au collisions at top RHIC energy [22]. For other beam energies the  $P_L/P_T$  ratio of baryons has become unity much earlier, and it achieves a constant value  $\sim 0.8$ – $0.7$  for  $t \geq 8$  fm/c at 20A GeV, for  $t \geq 7$  fm/c at 30A GeV and for  $t \geq 6$  fm/c at 40A GeV. On close inspection of Fig. 2, we found the pressure isotropization of non-strange baryons happen little earlier  $\Delta t \sim 0.5$  fm/c than strange baryons. The observation can be found in concurrence with an earlier UrQMD based calculation [23], which has shown the average freeze-out time of nucleons is smaller than the strange baryons ( $\Lambda, \Xi$ ). The  $P_L/P_T$  ratio of kaons approaches to 1.0 at early times  $t \sim 3$  fm/c and then becomes almost constant  $\sim 0.6$ – $0.7$  at the same time as the baryons. The initial longitudinal-to-transverse pressure (momentum) anisotropy of kaons has been found smaller than baryons, could be because of the facts that kaons have only one constituent quark from the orig-

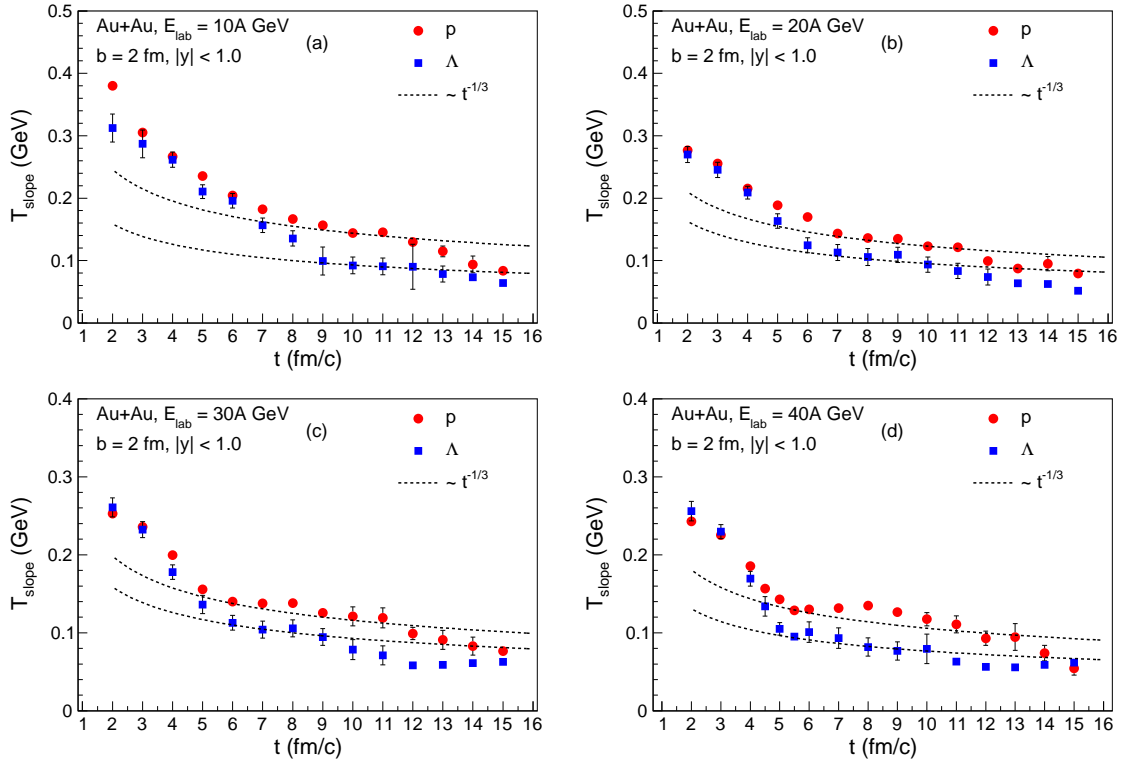


FIG. 3: (Color online) Time evolution of the inverse slope parameter ( $T_{slope}$ ) of the energy spectra of Proton and Lambda inside the central cell for Au+Au collisions ( $b = 2$  fm) at the laboratory energies (a) 10A, (b) 20A, (c) 30A, (d) 40A GeV. The error bars are statistical only.

inal excited hadron and suffer less resonant scatterings than baryons in medium. Thus we found the pressure isotropization time of baryons and mesons reduces by about 3 fm/c from  $E_{lab} = 10$  A GeV to  $E_{lab} = 40$  A GeV.

### C. Thermalization of energy spectra of baryons

In this section, we adopted an alternate approach to equilibrium which would reinforce the findings of earlier section. We investigated the time scale of local thermalization of baryonic matter from the time evolution of inverse slope parameter of the energy spectra ( $EdN/d^3p$  vs  $E$ ). For this purpose we have parameterized the energy spectra of Proton and Lambda inside the cell by Tsallis distribution [24]. An important criticism often arises that systems obeying non-extensive statistics achieve thermal equilibrium or not. Here we refer to the work of Bíró and Purcsel [25] which has shown that two non-extensive subsystems do achieve a common equilibrium distribution within the framework of non-extensive Boltzmann equation. The Tsallis

distribution has extensively been used in recent years for describing the transverse momentum ( $p_T$ ) distribution of produced hadrons at RHIC and the LHC energies [26, 27]. The special merit of the distribution is: at low energy limit it reduces to an exponential distribution and at high energy limit it reduces to a power-law distribution [28]. Thus it can accommodate both equilibrium and non-equilibrium phenomena. A recent work has found that Tsallis distribution fits reasonably good all particle spectra for  $p_T < 10$  GeV at midrapidity in d + Au, Cu + Cu, Au + Au collisions at RHIC [29]. Keeping the facts in mind, we write the energy spectra of Proton and Lambda inside the cell of dimension  $2 \times 2 \times 2$  fm<sup>3</sup> about the origin of Au + Au system as;

$$E \frac{d^3N}{d^3p} = C \left(1 + \frac{E}{bT}\right)^{-b}, \quad (3)$$

where  $E$  is the energy of baryon in the unit of GeV and  $b = 1/(q-1)$  is dimensionless.  $C$  has the unit of GeV<sup>-2</sup> and  $T$  is in GeV.  $q$  is called the non-extensive parameter of Tsallis distribution. The values of  $C$ ,  $b$ ,  $T$  are obtained through fitting the energy spectra up to  $E = 3$  GeV. The inverse slope parameter of

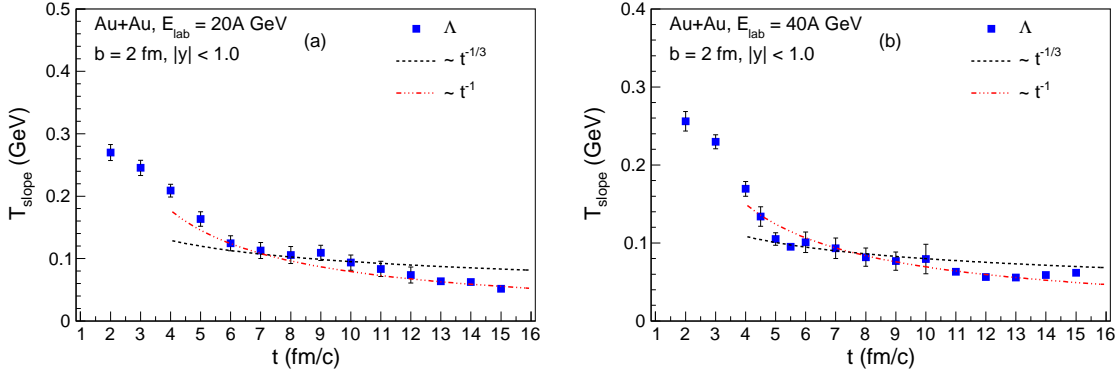


FIG. 4: (Color online) The scaling behaviour of inverse slope parameter ( $T_{slope}$ ) of the energy spectra of Lambda inside the central cell for Au+Au collisions ( $b = 2$  fm) at (a) 20A, (b) 40A GeV laboratory energies. The black dotted line denotes the scaling due to longitudinal expansion and the red dashed line denotes scaling due to three dimensional expansion. The error bars are statistical only.

this distribution is given by:

$$T_{slope} = T + (q - 1)E. \quad (4)$$

In the asymptotic limit  $E \rightarrow 0$ , the inverse slope parameter ( $T_{slope}$ ) gives the thermodynamic temperature of the system [25]. We have calculated the  $T_{slope}$  of proton and Lambda energy spectra at  $E = 0.1$  GeV (nearly pion mass) and studied its time evolution at the four beam energies. The error in  $T_{slope}$  arises from the errors in the fitting parameters  $T$  and  $b$ . The results are depicted in Fig. 3.

We have found  $T_{slope}$  (for Proton and Lambda both) falls sharply with time and then almost scales as  $\sim t^{-1/3}$  for  $t \gtrsim 9$  fm/c at 10A GeV laboratory energy. If  $T_{slope}$  corresponds to the local temperature of system, then we can infer an isentropic longitudinal expansion sets in inside the above mentioned cell analogous to Bjorken ideal hydrodynamics. The temperature follows the Bjorken scaling solution. We consider the time as the local thermal equilibration time scale of the system at which the scaling behaviour of the slope parameter has initiated. Similarly we have found the  $t^{-1/3}$  scaling holds good for  $t \gtrsim 7$  fm/c at 20A GeV,  $t \gtrsim 6$  fm/c at 30A GeV and for  $t \gtrsim 5$  fm/c at 40A GeV beam energy. At later times (say,  $t > 10$  fm/c at  $E_{lab} = 40A$  GeV), the  $T_{slope}$  is seen to scale as  $\sim t^{-1}$  owing to three dimensional spherical expansion of the system (see Fig. 4). The assumption of Bjorken hydrodynamic regime with the above mentioned scaling solution, namely, initial one-dimensional flow and ideal gas equation of state, could be dubious at lower collision energies. Although earlier works at AGS and SPS energies [30] have found phenomenological success based on it. However it may be noted that we do not study thermalization of whole reaction volume, rather concentrate at the very central part of

the system only. And for this region the above assumptions may be relevant, at least we can identify clearly the Bjorken scaling regime of  $T_{slope}$  for all energies (see Fig. 3). Thus we have found time scale of thermalization of energy spectra roughly in agrees with the pressure isotropization time of baryons and decreases with the increase in laboratory energy for the above mentioned cell.

A natural question about the analysis involving  $T_{slope}$  could arise that how better does the Tsallis distribution fit the spectrum compared to any classical distribution. In order to see that, we fit the energy spectra of baryons with Maxwell-Boltzmann (MB) distribution;  $f(E) = C' \exp(-(E - \mu)/T)$ .  $C'$  is a constant,  $T$  is the temperature and  $\mu$  is the chemical potential in usual notation. We have fitted the spectra for Au + Au collisions at  $E_{lab} = 30A$  GeV for the same range of  $E$  and calculated the chi-square per degrees of freedom ( $\chi^2/ndf$ ) for different times. The result is depicted in Fig. 5. It has been observed that Tsallis distribution mostly gives lower value of  $\chi^2/ndf$  which is close to unity in comparison to MB distribution. The inverse slope parameters of both distributions at different times are listed in Table I.

Several facts emerge upon close inspection. First, the two parameters are very similar at early times (say up to 3 fm/c). This might be due to numerical equivalence of the two distributions at these times. However it can be noted that  $\chi^2/ndf$  comes out very large at those times for both distributions; thus the parameters may not be describing a good fit.

Now in the thermal regime, say for  $t \geq 6$  fm/c, the two parameters differ by nearly 40 MeV and  $T_{slope}$  (Tsallis) is smaller than  $T$ (MB). The behaviour has been studied in the Ref. [31]. The Tsallis distribution describes a near-thermal equilibrium situation for  $q$  value close to unity. For the same particle

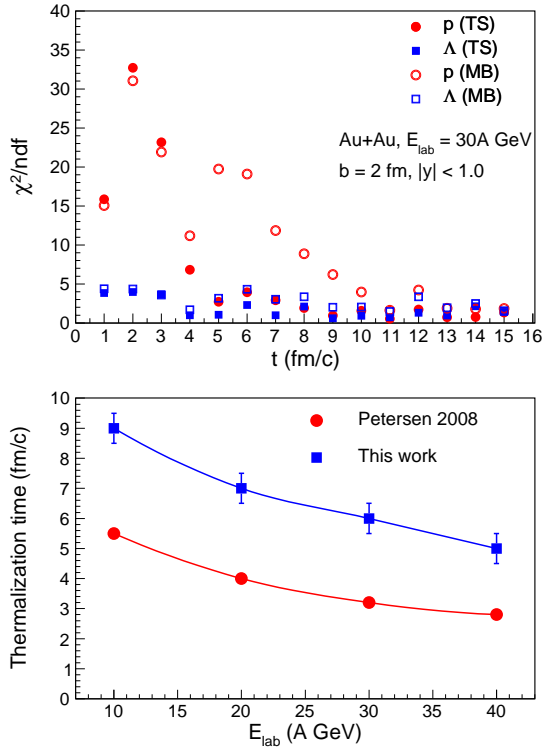


FIG. 5: (Color online) (Upper panel) The chi-square per degrees of freedom ( $\chi^2/ndf$ ) at different times for the Tsallis (filled symbols) and Maxwell-Boltzmann (open symbols) distribution which are fitted to the energy spectra of Proton and Lambda in the central cell for Au +Au collisions ( $b= 2$  fm) at  $E_{lab} = 30A$  GeV. (Lower panel) The thermalization time obtained in this work (blue square) is compared with the local thermalization time  $t_{start}$  (red circle) used in the hybrid (UrQMD + Hydrodynamics) model (Petersen 2008:[34]). The error bars are considered to be systematic.

yield, Tsallis distribution leads to lower temperature (i.e. inverse slope parameter) than MB distribution for  $q > 1$ . The Tsallis temperature often interpreted as the superposition different MB temperatures and the relative width of fluctuation in T(MB) is related to non-extensivity parameter  $(q - 1)$  [32]. We have checked that  $(q - 1)$  remains almost constant  $\sim 0.03$  during the time span. The constant difference between the slope parameters can be attributed to this fact. A similar trend between the inverse slope parameters has been reported in [33] where the particle spectra for central Pb-Pb collisions at the LHC energy, are fitted with both Tsallis and MB distribution.

#### D. A comparison with earlier work

We have compared our result with the local thermalization time scale ( $t_{start}$ ) used by an earlier work of hybrid model of Boltzmann transport and hydrodynamics by Petersen *et al.* [34]. The model has successfully described the data of rapidity dependent yield, transverse mass spectra of hadrons at AGS and SPS experiments. The  $t_{start}$  is considered ad hoc as the nuclear passage time in the center of mass frame. The comparison can be found in Fig. 5. We have introduced a systematic uncertainty of  $\pm 0.5$  fm in our estimated thermalization time because the simulation was carried out in time step  $\Delta t = 1$  fm. It has been found that our result decreases with increasing laboratory energy similar to  $t_{start}$  but is about 1.5 times larger in magnitude. The earlier work has assumed that  $t_{start}$  is the lowest possible time needed for local thermalization however the current study could provide a more realistic estimate of it. Nevertheless, the issue has been investigated further in Ref. [34] and found that multiplicity and mean transverse momenta of particles do not change appreciably when  $t_{start}$  increases by factor of 2.

#### IV. COMPARISON WITH STATISTICAL THERMAL MODEL

In the preceding sections we argued that the dense hadronic matter created in the collisions will achieve local thermal equilibrium on a certain time scale. Thus we can employ the statistical hadron gas model [35] to extract the intensive thermodynamic variables like; temperature, chemical potential of the system during subsequent evolution. The statistical model can not be applied prior to equilibrium, rather can be applied beyond thermal freeze-out of the system. Traditionally thermal freeze-out is defined as: the average scattering rate between the constituents becomes smaller than the average expansion rate of the system. The system has become so dilute that hardly any collision between the constituents takes place. Following this criterion, we have checked the time evolution of the average number of collisions ( $\langle N_{coll}(t) \rangle$ ) suffered by different hadron species. The Fig. 6 shows that average number of collisions suffered by p, n,  $\Lambda$ ,  $\Sigma$  baryons and  $K$  mesons almost saturate for  $t \gtrsim 17$  fm/c at  $E_{lab} = 10A$  GeV and  $t \gtrsim 15$  fm/c at  $E_{lab} = 30A$  GeV. Considering the above scenarios; we made the comparison of statistical model with UrQMD during the time interval  $10$  fm/c  $\leq t \leq 17$  fm/c at 10A GeV and  $8$  fm/c  $\leq t \leq 15$  fm/c at 30A GeV laboratory energy.

The expression for number density, energy density for the  $i$ 'th hadron species in the statistical hadron

| t    | $T_{slope}(Tsallis)$ | $T(MB)$ |
|------|----------------------|---------|
| fm/c | GeV                  | GeV     |
| 1    | 0.275                | 0.267   |
| 2    | 0.252                | 0.247   |
| 4    | 0.200                | 0.223   |
| 6    | 0.140                | 0.195   |
| 8    | 0.138                | 0.178   |
| 10   | 0.121                | 0.161   |
| 12   | 0.099                | 0.138   |
| 14   | 0.083                | 0.116   |

TABLE I: The inverse slope parameters for Tsallis and Maxwell-Boltzmann distributions at different times. The distributions are fitted to the energy spectra of Protons in the central cell for Au+Au collisions at  $E_{lab} = 30A$  GeV.

| $E_{lab} = 10A$ GeV |       |         |         | $E_{lab} = 30A$ GeV |       |         |         |
|---------------------|-------|---------|---------|---------------------|-------|---------|---------|
| t                   | T     | $\mu_B$ | $\mu_s$ | t                   | T     | $\mu_B$ | $\mu_s$ |
| fm/c                | GeV   | GeV     | GeV     | fm/c                | GeV   | GeV     | GeV     |
| 10                  | 0.145 | 0.708   | 0.174   | 8                   | 0.152 | 0.616   | 0.123   |
| 11                  | 0.136 | 0.697   | 0.148   | 9                   | 0.145 | 0.601   | 0.100   |
| 12                  | 0.128 | 0.687   | 0.125   | 10                  | 0.137 | 0.595   | 0.081   |
| 13                  | 0.120 | 0.680   | 0.102   | 11                  | 0.129 | 0.593   | 0.067   |
| 14                  | 0.114 | 0.670   | 0.082   | 12                  | 0.123 | 0.587   | 0.047   |
| 15                  | 0.108 | 0.664   | 0.070   | 13                  | 0.115 | 0.586   | 0.031   |
| 16                  | 0.102 | 0.659   | 0.049   | 14                  | 0.110 | 0.586   | 0.019   |
| 17                  | 0.097 | 0.656   | 0.041   | 15                  | 0.105 | 0.585   | 0.011   |

TABLE II: The time evolution of temperature (T), baryon chemical potential( $\mu_B$ ), strange chemical potential ( $\mu_s$ ) in the central cell ( $2 \times 2 \times 2$  fm<sup>3</sup>) for Au + Au collisions (b = 2 fm) at laboratory energies 10A and 30A GeV. The thermodynamic parameters are obtained from energy density of baryons ( $\varepsilon_B$ ), number density of baryons ( $n_B$ ) and number density of strange hadrons ( $n_s$ ) using statistical hadron gas model.

gas model are given by:

$$n_i = \frac{g_i}{(2\pi\hbar)^3} \int 4\pi p^2 f_i(T, \mu_i) dp,$$

$$\varepsilon_i = \frac{g_i}{(2\pi\hbar)^3} \int 4\pi p^2 e_i f_i(T, \mu_i) dp,$$

where  $e_i$  is the energy,  $T$  is the temperature and  $\mu_i$  is chemical potential of the  $i$ 'th hadron. The hadrons are considered relativistic,  $e_i = (p^2 + m_i^2)^{\frac{1}{2}}$ .  $f_i$  is the distribution function of the  $i$ 'th hadron (either Fermi-Dirac or Bose-Einstein). However above distributions are practically approximated to classical MB distribution as;  $(e_i - \mu_i)/T \gg 1$ .  $\mu_i$  can be decomposed in terms of baryonic ( $\mu_B$ ) and strange ( $\mu_s$ ) chemical potentials. The charge chemical potential ( $\mu_Q$ ), which is an order of magnitude smaller than the other two, has been neglected here.

$$\mu_i = b_i \mu_B + s_i \mu_s,$$

$b$  and  $s$  are the baryon and strangeness quantum number respectively.  $T$ ,  $\mu_B$ , and  $\mu_s$  are extracted

from the following equations;

$$\varepsilon_B = \sum_i^{baryon} \varepsilon_i, \quad n_B = \sum_i^{baryon} b_i n_i, \quad n_s = \sum_i^{baryon, meson} s_i n_i \quad (5)$$

The quantities in the l.h.s. of the equation 5, namely energy density of baryons ( $\varepsilon_B$ ), number density of baryons ( $n_B$ ) and number density of strange hadrons ( $n_s$ ) are obtained from the UrQMD. We have solved the above set of equations during the time interval stated earlier. The values are listed in Table II. We have plotted them in the QCD phase diagram in order to get an estimate about the chemical and thermal freeze-out time of the system (see Fig. 7). The chemical freeze-out line has been obtained empirically from the thermal model fit of particle ratios at different collision energies [36]. The thermal or kinetic freeze-out line has also been obtained phenomenologically from the blast wave model fits of the measured hadron spectra at different experiments [37]. It can be seen at low energies  $E_{lab} = 10A$  GeV, the chemical and the kinetic freeze-out happens almost instantaneously at  $t \approx 17$  fm/c.



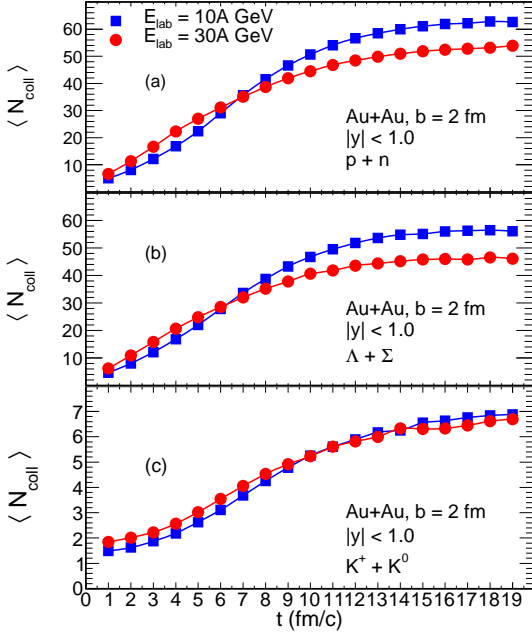


FIG. 6: (Color online) Time evolution of average number of collisions ( $\langle N_{coll}(t) \rangle$ ) suffered by (a) Protons and Neutrons, (b) Lambda and Sigma baryons, (c) Kaons for Au + Au collisions ( $b = 2$  fm) at laboratory energies 10A and 30A GeV.

At higher energy  $E_{lab} = 30$  A GeV, system undergoes first chemical freeze-out at  $t \approx 13$  fm/c, then kinetic freeze-out at  $t \approx 15$  fm/c. The feature has already observed in low energy collision experiments at RHIC [38]. We would also like to add that our estimation of temperatures at the kinetic freeze-out times closely agree with the values given by blast wave model fit to the  $\Lambda$  baryon spectra from NA49 Collaboration at the similar laboratory energies [15].

We are interested in computing bulk properties of a baryon rich hadronic medium, thus strange meson contribution can be neglected as  $\mu_s \rho_M^S \approx$  few MeV. Using the values of temperature and chemical potential listed in Table II, we have calculated the pressure of baryons with the statistical hadron gas model:

$$P = \sum_i^{baryon} \frac{g_i}{(2\pi\hbar)^3} \int 4\pi p^2 dp \frac{p^2}{3(p^2 + m_i^2)^{\frac{1}{2}}} f_i(T, \mu_i), \quad (6)$$

and the entropy density ( $s$ ) for baryons using the thermodynamic relation:

$$Ts = \varepsilon_B + P - \mu_i(\rho_B^{NS} + \rho_B^S), \quad (7)$$

where  $\mu_i$  is the chemical potential, defined earlier in this section. We studied the time evolution of

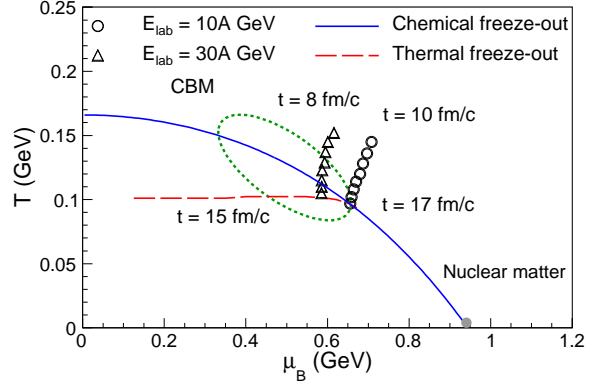


FIG. 7: (Color online) The evolution of temperature ( $T$ ) and baryo-chemical potential ( $\mu_B$ ) in the central cell for Au + Au collisions ( $b = 2$  fm) at  $E_{lab} = 10$  A GeV and 30A GeV. The solid (blue) line denotes the chemical freeze-out and the dashed (red) line denotes thermal freeze-out boundary in relativistic heavy ion collisions [36, 37]. The dotted circle denotes the expected region probed by the CBM experiment ( $\sqrt{s_{NN}} = 4-10$  GeV) at FAIR.

entropy density at  $E_{lab} = 10$  A and 30A GeV till the thermal decoupling. Our aim is to get some insight about the fluidity of the dense baryonic matter created in these collisions. In recent times several calculations [39–41] have been reported on the transport properties of hadronic matter at finite baryo-chemical potential, including the effect high mass resonances, etc. However the fluidity of dense hadronic matter has possibly first discussed in [40] and subsequently in [42, 43]. The authors of Ref. [40] have argued that the fluid behaviour of a baryon rich ( $\mu_B \sim 500$  MeV) hadron gas is closer to the ideal fluid limit than the corresponding gas with zero baryon number. Following their observation, we have compared the entropy densities at  $E_{lab} = 10$  A and 30A GeV with the ideal fluid limit reached at the highest RHIC energy ( $\sqrt{s_{NN}} = 200$  GeV). We have parameterized temporal evolution of entropy density of hadronic matter from an ideal hydrodynamic simulation [44] for central Au + Au collisions at  $\sqrt{s_{NN}} = 200$  GeV. The entropy density at  $r = 3$  fm from the center has been found to scale with proper time ( $\tau$ ) as  $\sim \tau^{-2.6}$  for  $\tau \geq 10$  fm/c. The results are depicted in Fig. 8 along with the parameterization from ideal hydrodynamics. It is heartening to see that the evolution of entropy density at  $E_{lab} = 30$  A GeV closely resembles with ideal hydrodynamic limit at zero net baryon density. The entropy density at  $E_{lab} = 10$  A GeV falls even little faster than the aforementioned limit. It may imply that the hadronic matter produced at 10A GeV beam energy is more ideal than the same at 30A GeV beam energy. The observation

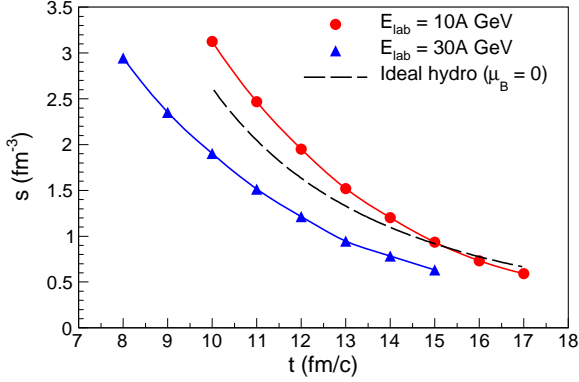


FIG. 8: (Color online) The time evolution of entropy density of baryonic matter inside the central cell for Au + Au collisions ( $b = 2$  fm) at  $E_{\text{lab}} = 10\text{A}$  GeV and  $30\text{A}$  GeV. The dashed line denotes the parameterization of ideal hydrodynamic evolution of entropy density in the central region for Au + Au collisions ( $b = 0$  fm) at  $\sqrt{s_{NN}} = 200$  GeV [44].

can be understood using the fact that shear viscosity to entropy density ratio ( $\eta/s$ ) of a hadronic system decreases with increasing fugacity ( $\mu_B/T$ ) of the system [21].

## V. SUMMARY AND DISCUSSION

In this article, we have investigated the time scale for local thermal equilibration of dense baryonic matter created in central Au + Au collisions at the proposed CBM experiment energies of  $E_{\text{lab}} = 10\text{A}, 20\text{A}, 30\text{A}, 40\text{A}$  GeV. The microscopic transport model UrQMD has been used for this purpose in the default cascade mode. The net baryon density has been found maximum at 30-40 GeV and the net strangeness of the created hadronic matter is dominated by baryons for all energies stated above. We have studied the time evolution of longitudinal-

to-transverse microscopic pressure anisotropy and inverse slope parameter of the energy spectra of baryons and mesons inside a cell of  $8\text{ fm}^3$  in the central region of Au + Au system. The pressure anisotropy ratio of baryons and mesons has achieved a constant value close to unity, on a certain time. The time has been found to decrease with the increase in laboratory energy. The time scale obtained from the evolution of inverse slope parameter of energy spectra of baryons nearly agrees with the pressure (or momentum) isotropization time. However a small time difference ( $\Delta t \sim 0.5\text{ fm/c}$ ) in the pressure isotropization as well as in the thermalization of energy spectra between strange and non-strange baryons has been noticed. We have chosen our test volume in the central collision zone. The estimated time scales are expected to grow in a region which is away from the center because of small scattering rates. Therefore the present study provides a realistic estimate of the time scales required for achieving thermodynamic equilibrium for the central region of the system created at those energies.

Using the statistical thermal model, we have obtained the temperature and chemical potentials of the hadronic matter during the post-equilibrium evolution at  $E_{\text{lab}} = 10\text{A}$  and  $30\text{A}$  GeV. They are found to agree qualitatively with the empirical relation between  $T$  and  $\mu_B$  at the chemical freeze-out. In addition we have calculated the entropy density of the baryonic matter inside the cell and found the evolution is quasi-isentropic, close to the ideal hydrodynamic limit at zero net baryon density.

## VI. ACKNOWLEDGEMENT

The work is partially supported by Bose Institute Indo-Fair Coordination Centre (BI-IFCC). We are thankful to Grid tier-2 center, Kolkata for providing computing resources. We acknowledge the financial assistance from DAE, India and FAPESP, Brasil, during the course of the work.

- 
- [1] B. B. Back *et al.*, Nucl. Phys. A **757**, 28 (2005).  
[2] N. Armesto *et al.*, J. Phys. G **35**, 054001 (2008).  
[3] O. Philipsen, Prog. Part. Nucl. Phys. **70**, 55 (2013).  
[4] N. Xu (STAR Collaboration), Nucl. Phys. A **931** 1 (2014).  
[5] S. Chattopadhyay, J. Phys. G **35**, 104027 (2008).  
[6] B. Friman *et al.* : The CBM Physics Book, Lect. Notes Phys. 814, Springer-Verlag Berlin Heidelberg (2010).  
[7] P. Senger, Prog. in Part. and Nucl. Phys. **62**, 375 (2009).  
[8] V. I. Kolesnikov and A. I. Zinchenko, arXiv:1312.1091 [nucl-ex].  
[9] H. R. Schmidt (CBM Collaboration), PoS (Bormio 2013) 061.  
[10] R. Baier, A. H. Mueller, D. Schiff and D. T. Son, Phys. Lett. B **502**, 51 (2001).  
[11] F. Gelis, Nucl. Phys. A **931**, 73 (2014).  
[12] S. A. Bass *et al.*, Prog. Part. Nucl. Phys. **41**, 225 (1998); M. Bleicher *et al.*, J. Phys. G **25**, 1859 (1999).  
[13] W. Cassing, E. L. Bratkovskaya and S. Juchem, Nucl. Phys. A **674**, 249 (2000).  
[14] Z. W. Lin, C. M. Ko, B. A. Li, B. Zhang and S. Pal,

- Phys. Rev. C **72**, 064901 (2005).
- [15] C. Alt *et al.* (NA49 Collaboration), Phys. Rev. C **78**, 034918 (2008).
- [16] J. Cugnon, Phys. Rev. C **22**, 1885 (1980).
- [17] I. C. Arsene *et al.*, Phys. Rev. C **75**, 034902 (2007).
- [18] B. Friman, W. Norenberg and V. D. Toneev, Eur. Phys. J. A **3**, 165 (1998).
- [19] G. Q. Li, C. H. Lee and G. E. Brown, Nucl. Phys. A **625**, 372 (1997).
- [20] L. V. Bravina *et al.*, Phys. Lett. B **434**, 379 (1998).
- [21] N. Demir and S. A. Bass, Phys. Rev. Lett. **102**, 172302 (2009).
- [22] M. Ruggieri *et al.*, Phys. Rev. C **89**, 054914 (2014).
- [23] Z. Xie, P. Ning and S. A. Bass, J. Phys. G **37**, 045002 (2010).
- [24] C. Tsallis, J. Statist. Phys. **52**, 479 (1988).
- [25] T. S. Bíró and G. Purcsel, Phys. Lett. A **372**, 1174 (2008).
- [26] J. Cleymans and D. Worku, Eur. Phys. J. A **48**, 160 (2012).
- [27] P. K. Khandai, P. Sett, P. Shukla and V. Singh, J. Phys. G **41**, 025105 (2014).
- [28] C. Y. Wong and G. Wilk, Acta. Phys. Polon. B **43** 2047 (2012).
- [29] H. Zheng and Lilin Zhu, Advances in High Energy Physics, vol. 2015, Article ID 180491, 2015.
- [30] P. F. Kolb, J. Solfrank, U. Heinz, Phys. Lett. B **459**, 667 (1999); H. Dobler, J. Solfrank, U. Heinz, Phys. Lett. B **457**, 353 (1999).
- [31] J. Cleymans, G. Hamar, P. Levai and S. Wheaton, J. Phys. G **36** 064018 (2009).
- [32] G. Wilk and Z. Włodarczyk, Phys. Rev. Lett. **84**, 2770 (2000).
- [33] F. H. Liu, Y. Q. Gao and B. C. Li, Eur. Phys. J. A **50**, 123 (2014).
- [34] H. Petersen *et al.*, Phys. Rev. C **78**, 044901 (2008).
- [35] P. Braun-Munzinger, K. Redlich and J. Stachel, nucl-th/0304013.
- [36] J. Cleymans, H. Oeschler, K. Redlich and S. Wheaton, Phys. Rev. C **73**, 034905 (2006).
- [37] U. W. Heinz, arXiv:0901.4355 [nucl-th] and references therein.
- [38] B. Mohanty, Nucl. Phys. A **830**, 899C (2009).
- [39] K. Itakura, O. Morimatsu and H. Otomo, Phys. Rev. D **77**, 014014 (2008).
- [40] G. S. Denicol, C. Gale, S. Jeon and J. Noronha, Phys. Rev. C **88**, 064901 (2013).
- [41] G. P. Kadam and H. Mishra, Nucl. Phys. A **934**, 133 (2014).
- [42] S. Ghosh, Phys. Rev. C **90**, 025202 (2014).
- [43] G. P. Kadam and H. Mishra, Phys. Rev. C **92**, 035203 (2015).
- [44] P. F. Kolb and U. Heinz, nucl-th/0305084.